Available online at www.sciencedirect.com
SCIENCE DIRECT®
PERGAMON
International Journal of Rock Mechanics & Mining Sciences 40 (2003) 377–387
International Journal of Rock Mechanics and Mining Sciences
www.elsevier.com/locate/ijrmms

Rayleigh wave propagation in intact and damaged geomaterials

M. Stavropoulou[a], G. Exadaktylos[b,*], E. Papamichos[c], I. Larsen[c], C. Ringstad[c]

[a] *Section of Mechanics, Department of Engineering Science, National Technical University of Athens, 5 Heroes of Polytechnion Av, GR-15773 Athens, Greece*

[b] *Mine Design Laboratory, Department of Mineral Resources Engineering, Technical University of Crete, Hania GR-73100, Greece*

[c] *SINTEF Petroleum Research, N-7034 Trondheim, Norway*

Accepted 11 January 2003

Abstract

An analytical model of an elastically deforming geomaterial with microstructure and damage is assumed to be a material where the second spatial gradients of strain are included in the constitutive equations. Based on this assumption, a linear second gradient (or grade-2) elasticity theory is employed, to investigate the propagation of surface waves in either intact or weathered—although homogeneous and isotropic at the macroscale—materials with microstructure such as soils, rocks and rock-like materials. First, it is illustrated that in contrast to classical (grade-1) elasticity theory, the proposed higher-order elasticity theory yields dispersive Rayleigh waves, as it is also predicted by the atomic theory of lattices (discrete particle theory), as well as by viscoleasticity theory. Most importantly, it is demonstrated that the theory: (a) is in agreement with in situ non-destructive measurements pertaining to velocity dispersion of Rayleigh waves in monumental stones, and (b) it may be used for back analysis of the test data for the quantitative characterization of degree of surface cohesion or damage of Pendelikon marble of the Parthenon monument of Athens.

1. Introduction

Fig. 1a and b show the damage exhibited by the marble at the mesoscopic scale (in which the representative volume element is the grain size) produced during unconfined compression fatigue tests on Dionysos marble specimens [1]. This damage is manifested by calcite grain decohesion and transgranular microcracking (Fig. 1a). In greater detail (Fig. 1b) fine fragments a few microns wide, which accumulate in the proximity of the grain corners may be observed. Obviously, this damage results to an inhomogeneous strain field even if the grains have the same properties and great care has been taken to obtain a uniform strain field inside the marble specimen.

Speaking in terms of lattice dynamics, classical elasticity has been developed on the assumption of the "nearest-neighbor interaction" and does not consider the interaction between imperfections, hence the term "local" theory. One way to include in a continuum model "non-local" stresses being due to imperfection interactions is by assuming that the stress at a point of the medium is a function of the strain at that point, as well as additional space derivatives of the strain there. The results are an inhomogeneous strain field in a problem where the classical approach produces uniform strain.

In this paper, a linear gradient elasticity theory is employed to investigate the propagation of surface waves in a homogeneous (at the macroscopic level) half-space with polycrystalline or granular structure (e.g. geomaterials or rock-like materials) that may exhibit some degree of damage. This theory may be considered a special case of the general Mindlin's theory [2] of a second strain-gradient linear elasticity with microstructure. In particular, the theory assumes a strain-energy density expression including, besides the classical terms, strain-gradient terms and introduces also a microstress (which works on the strain), a double stress (which works on the strain gradient), and a total stress obeying the momentum balance equations. Within this formulation, two characteristic internal length scales of the medium are introduced. One of them is associated with an additional term appearing in the strain-energy

*Corresponding author. Tel.: +30-28210-37650; fax: +30-28210-69554.
E-mail address: exadakty@mred.tuc.gr (G. Exadaktylos).

1365-1609/03/$ - see front matter
doi:10.1016/S1365-1609(03)00012-1

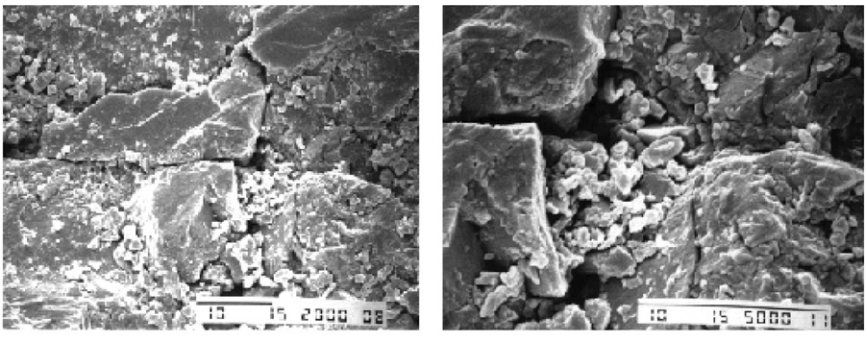

(a) (b)

Fig. 1. Outer surface of partially loaded Dionysos marble (a) at 2000 × magnification (b) Partially-loaded specimen outer surface at 5000 × magnification [1].

density expression and accounts for the strain gradients. The other is the characteristic size of the unit cell of the medium (i.e. crystallite of a polycrystalline rock or grain of a granular soil or rock material). Such a theory of elasticity has been successfully employed in [3–10] to revisit basic problems in Fracture Mechanics, Rock Mechanics and Theory of Elasticity. In these works it was shown that this enhanced elasticity theory is capable to: (a) predict size effect of strength, (b) eliminate strain singularities in crack tips and in half-planes under concentrated forces, and (c) to predict cusp-like instead of elliptical crack profiles. It has also been shown in [11] that the new theory is capable of predicting SH surface waves, that is anti-plane shear motions exponentially decaying with the distance from the free surface, which of course is in contrast with the expectations of the classical elasticity theory. It is noted here that even the non-local linear elasticity theory of Eringen [12,13], which certainly proved successful in treating several other problems, is not capable of predicting surface SH waves (see e.g. [14]). In another paper [15], it was the first time that it was shown that the form of the dispersion relation of surface SH waves predicted by the gradient theory, resembles that found by Coulson [16] for surface waves in liquids that possess surface energy. Also, in a recent paper [17] the classical plane stress/strain problem of Rayleigh wave propagation was revisited within the framework of gradient elasticity. Contrary to the classical result, it was found that this wave exhibits either normal or anomalous dispersion, a fact that is in agreement with experimental evidence referring to preliminary in situ non-destructive surface wave measurements in the Parthenon of Acropolis of Athens.

In this work it is shown that the theory may be used for back analysis of the in situ non-destructive surface wave test results for the quantitative characterization of degree of surface cohesion and damage of monumental Dionysos–Pendelikon marble of the Parthenon monument of Athens.

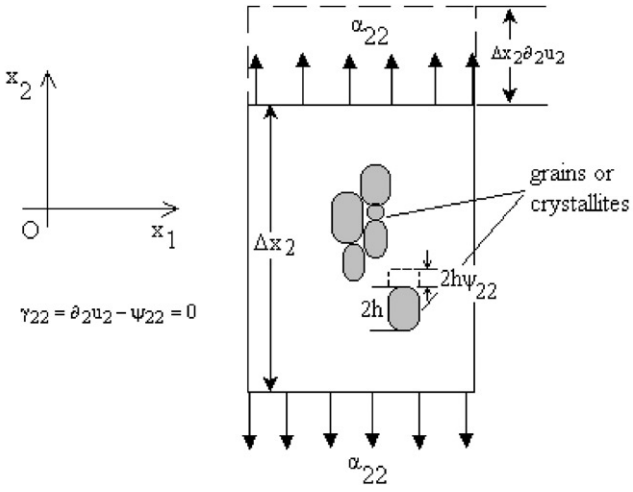

Fig. 2. Typical components of relative stress α_{ij} ($\alpha_{ij} \equiv \sigma_{ij} - \tau_{ij}$,) displacement gradient $\partial_i u_j$, micro-deformation ψ_{ij} and relative deformation γ_{ij} for the simple case of uniaxial tension.

2. Basic equations of grade-2 elasticity theory and the physical meaning of the length scales

In this section, we briefly outline the basic equations of the grade-2 theory employed to analyze time—harmonic surface wave motions. With respect to a Cartesian coordinate system $Ox_1x_2x_3$, the following *ansatz* for the strain-energy density with respect to the kinematic quantities is assumed

$$W = W(\varepsilon_{qr}, \kappa_{qrs}), \tag{1}$$

where $\varepsilon_{qr} \equiv (1/2)(\partial_r u_q + \partial_q u_r)$ is the usual symmetric infinitesimal strain tensor defined in terms of the displacement vector u_q, $\partial_s \equiv \partial/\partial x_s$, the indices (q, r, s) span the range (1,2,3), and $\kappa_{qrs} \equiv \partial_q \psi_{rs}$ is the micro deformation gradient in which ψ_{qr} denotes the micro deformation (Fig. 2). Then, appropriate definitions for the stresses follow from the variation of W, i.e.

$$\tau_{qr} \equiv \frac{\partial W}{\partial \varepsilon_{qr}}, \qquad \mu_{qrs} \equiv \frac{\partial W}{\partial \kappa_{qrs}}, \tag{2}$$

in which (τ_{qr}, μ_{qrs}) are the microstress (symmetric), and the double-stress tensors, respectively. Further, from the variational equation of motion (by taking independent variations δu_q and $\delta\psi_{qr}$), one may obtain 12 stress equations of motion and 12 traction boundary conditions. These equations of a linear continuum with microstructure [2] contain the equations of a Cosserat linear continuum as a special case.

In particular, the theory utilized here can be considered one of the simplest versions of Mindlin's theory corresponding to the following strain-energy density function of an isotropic grade-2 elastic material [10]

$$W = (1/2)\lambda\varepsilon_{qq}\varepsilon_{rr} + G\varepsilon_{qr}\varepsilon_{rq} + G\ell^2(\partial_s\varepsilon_{qr})(\partial_s\varepsilon_{rq}), \tag{3}$$

where $\lambda = Ev/(1-2v)(1+v)$ and $G = E/2(1+v)$ are the standard constants of Lame, E is Young's modulus, v is Poisson's ratio and ℓ is the strain gradient coefficient (having dimensions of (length)). One may notice that the theory approaches the local elasticity theory in the limit $\ell = 0$. It may also be proved that positive definiteness of the strain-energy density requires the following restrictions of the material constants

$$(3\lambda + 2G) > 0, \quad G > 0, \quad \ell^2 > 0. \tag{4}$$

The last inequality simply means that ℓ should be a real and not imaginary number. The stress equation of motion reads as follows:

$$\partial_q\sigma_{qr} = \rho\ddot{u}_r, \tag{5}$$

where σ_{qr} denotes the symmetric total stress tensor defined as follows:

$$\sigma_{qr} = \tau_{qr} - \partial_k\mu_{kqr} + \tfrac{1}{3}\rho h^2\nabla^2\ddot{u}_r, \tag{6}$$

where the last term of the r.h.s. of Eq. (6) refers to the effect of micro-inertia of solid grains. We remark here that σ_{qr} may be considered as the Cauchy stress tensor with the associated Cauchy traction or stress vector t_r defined by

$$t_r \equiv n_q\sigma_{qr}. \tag{7}$$

This stress vector is employed for the specification of "traction" boundary conditions. These conditions must be supplemented with the double traction boundary conditions

$$m_r = n_q n_s \mu_{qsr}, \tag{8}$$

where n_s are the components of the unit vector outnormal to the boundary, t_r is the surface force per unit area, and m_r is the surface double force (without moment).

Finally, the constitutive equations for the stresses follow by combining Eqs. (2) and (3)

$$\begin{aligned}\tau_{qr} &= \lambda\delta_{qr}\varepsilon_{ss} + 2G\varepsilon_{qr},\\ \sigma_{qr} &= \lambda\delta_{qr}\varepsilon_{kk} + 2G(\varepsilon_{qr} - \ell^2\nabla^2\varepsilon_{qr})\\ &\quad + (1/3)\rho h^2(\partial_q\ddot{u}_r),\\ \mu_{sqr} &= 2G\ell^2\partial_s\varepsilon_{qr}.\end{aligned} \tag{9}$$

From the last of the above relations we may note that the double stress is symmetric in the last two indices.

The physical significance of the strain-gradient length scale ℓ—that is the length scale associated with the strain gradient $(\partial_s\varepsilon_{qr})$—is demonstrated by virtue of an example from Fracture Mechanics. For this purpose we consider the simplest case of the anti-plane shear (mode-III) crack. In contrast to Griffith's approach, the effect of cohesive forces on the displacements and strains is taken into account in this theory by including higher-order gradients in the constitutive equations. For this purpose let us consider a homogeneous isotropic microelastic medium uninterrupted except for the mode-III crack occupying the line segment $-\alpha < x < \alpha$, $y = 0$ with traction-free faces. The body is subjected to a constant shear traction $\sigma_{yz} = \tau_\infty$ at infinity. The approximate solution for mode-III crack has as follows [18].

$$\begin{aligned}u_z \cong \left(\frac{\tau_\infty}{G}\right)\frac{\ell^{-2}}{5806080}\{&-5083\alpha^6 + 1866x^2\alpha^4 - 264x^4\alpha^2\\ &+ 16x^6 + 29376\ell^2\alpha^4 - 10368x^2\alpha^2\ell^2 + 1152x^4\ell^2\\ &-169344\ell^4\alpha^2 + 48384x^2\ell^4 + 967680\ell^6\}\\ &\times(\alpha^2 - x^2)^{3/2}, \quad 0 \leqslant x < \alpha, \quad \ell > \sqrt{2}\alpha.\end{aligned} \tag{10}$$

Fig. 3 displays the crack shapes obtained from Eq. (10) for $\ell/\alpha = 0.7, 0.8, 0.9, 1$ with the crack displacements lower for higher ℓ/α values.

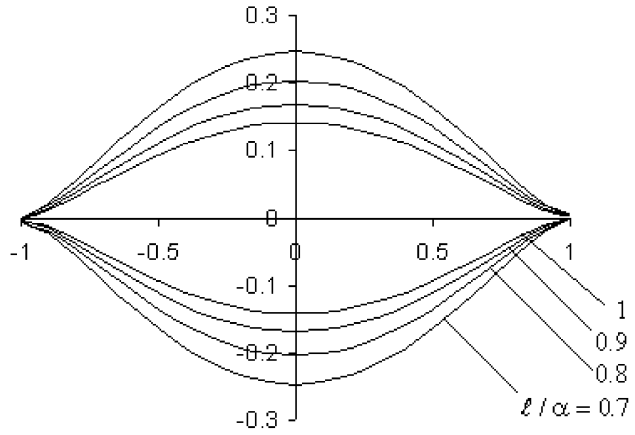

Fig. 3. Normalized crack face displacements $u_z/(\tau_\infty/G)$ predicted by the present strain-gradient theory for four values of the relative length at hand and for $\alpha = 1$.

Thus, the physical significance of the lengthscale ℓ for given crack length is to control the stiffness of the crack. In other words, as the internal length ℓ increases with respect to the crack length of a given material, the cohesion of the material increases, hence strain gradient elasticity theory may be called "cohesive elasticity theory".

Finally, it may be remarked that the asymptotic expansion of the crack displacement close to crack tip at $y=0$ takes the following cusp—form due to cohesive forces that act at the crack tip region

$$u_z|_{x\to 0} \cong \frac{\tau_\infty \sqrt{2\alpha}}{G\ell}\left(x^{3/2} - \frac{1}{2\ell}\, x^{5/2} + o\left[x^{7/2}\right]\right), \tag{11}$$

in which $o[\cdot]$ denotes the order-of-magnitude symbol. It is worth noting that classical fracture mechanics predicts elliptical crack profile with $u_z|_{x\to 0} \propto x^{1/2}$ close to the crack tip. This is due to the fact that elasticity ignores the effect of cohesive forces that act at the crack tip region. From the above formula a new material parameter may be defined as the product $G\ell$ with dimensions $[F\cdot L^{-1}]$, where F denotes force and L denotes length. Herein this new parameter is called "crack stiffness" and below it is demonstrated that it may be experimentally determined through carefully performed Rayleigh wave in situ tests.

3. Propagation of Rayleigh surface waves

The possibility of a wave travelling along the free surface of an elastic half-space, under conditions of plane strain, such that the disturbance is largely confined to the neighborhood of the boundary was first considered by Lord Rayleigh [19]. The classical theory of linear elasticity predicts no dispersion for these motions; only including viscoelastic [20] or thermoelastic [21] effects in the constitutive behavior leads to *dispersive* Rayleigh waves. Moreover, in order to explain the occurrence of dispersion of Rayleigh waves, Vardoulakis [22] has considered a graded half-space, that is a material with stiffness increasing with depth. Here, as it was mentioned above, we take another path of thought and consider the propagation of Rayleigh waves in a gradient elastic, macrohomogeneous and isotropic half-space $x_2 \leqslant 0$ (Fig. 4) having as an objective of examining the possibility of dispersive behavior.

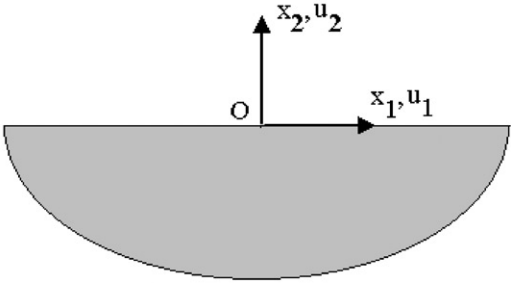

Fig. 4. Half-space and coordinates.

The boundary conditions for the problem at hand by requiring that the total stress tensor defined by Eq. (7) and the double traction tensor defined by Eq. (8) to vanish at the free surface. Hence, along the planar boundary of the half-plane the conditions take the form respectively,

$$\begin{aligned} &\sigma_{22} = \sigma_{21} = 0, \quad \mu_{222} = \mu_{221} = 0, \\ &\quad -\infty < x_1 < \infty, \quad x_2 = 0. \end{aligned} \tag{12}$$

By considering steady-state harmonic vibrations, i.e.

$$u_i = \bar{u}_i e^{i\omega t}, \tag{13}$$

in which ω denotes the cyclic frequency of the wave, and $i \equiv \sqrt{-1}$ is the usual imaginary unit, we obtain the solution of the displacement field, which in turn is substituted into the second and third of the constitutive equations (9) in order to arrive at the total stress and double-stress fields, respectively. Then, the appropriate dispersion or frequency equation is obtained by enforcing the traction and double traction boundary conditions (7) and (8), respectively, along the half-space surface $x_2 = 0$, i.e.

$$\begin{aligned} \sigma_{22}/(G\hat{\beta}^2 e^{i\hat{\beta}x} e^{i\omega t}) &= \left\{-a + \left[(a+2) - 2\hat{\beta}^2(Z_1^2 - 1)\right.\right. \\ &\quad \left.\left. + 2\hat{\beta}^2 - \tfrac{1}{3}\hat{h}^2\Omega^2\right] Z_1^2\right\} A_1 \\ &\quad + \left\{-a + \left[(a+2) - 2\hat{\beta}^2(Z_2^2 - 1)\right.\right. \\ &\quad \left.\left. + 2\hat{\beta}^2 - \tfrac{1}{3}\hat{h}^2\Omega^2\right] Z_2^2\right\} A_2 \\ &\quad + i\left[2 - 2\hat{\beta}^2(Z_3^2 - 1) - \tfrac{1}{3}\hat{h}^2\Omega^2\right] Z_3 A_3 \\ &\quad + i\left[2 - 2\hat{\beta}^2(Z_4^2 - 1) - \tfrac{1}{3}\hat{h}^2\Omega^2\right] Z_4 A_4 = 0, \\ \sigma_{21}/(G\hat{\beta}^2 e^{i\hat{\beta}x} e^{i\omega t}) &= i\left[-2 - 2\hat{\beta}^2(1 - Z_1^2) - \hat{\beta}^2 + \tfrac{1}{3}\hat{h}^2\Omega^2\right] Z_1 A_1 \\ &\quad + i\left[-2 - 2\hat{\beta}^2(1 - Z_2^2) - \hat{\beta}^2 + \tfrac{1}{3}\hat{h}^2\Omega^2\right] Z_2 A_2 \\ &\quad + \left[1 + Z_3^2(1 - \hat{\beta}^2) + \hat{\beta}^2(1 - Z_3^4) - \tfrac{1}{3}\hat{h}^2\Omega^2 Z_3\right] A_3 \\ &\quad + \left[1 + Z_4^2(1 - \hat{\beta}^2) + \hat{\beta}^2(1 - Z_4^4) - \tfrac{1}{3}\hat{h}^2\Omega^2 Z_4\right] A_4 \\ &= 0 \end{aligned} \tag{14}$$

and

$$\begin{aligned} \mu_{222}/(2G\ell\hat{\beta} e^{i\hat{\beta}x} e^{i\omega t}) &= -\hat{\beta}^2[Z_1^3 A_1 + Z_2^3 A_2] - i\hat{\beta}^2[Z_3^2 A_3 + Z_4^2 A_4] = 0, \\ \mu_{221}/(-G\ell\hat{\beta} e^{i\hat{\beta}x} e^{i\omega t}) &= -2i\hat{\beta}^2[Z_1^2 A_1 + Z_2^2 A_2] + \hat{\beta}^2[(1 + Z_3^2)Z_3 A_3 \\ &\quad + (1 + Z_4^2)Z_4 A_4] = 0. \end{aligned} \tag{15}$$

In the above equations we have set the following dimensionless variables

$$\hat{\beta} = \ell\beta, \quad x = x_1/\ell, \quad y = x_2/\ell,$$
$$a = \frac{2\nu}{1-2\nu}, \quad \hat{h} = \frac{h}{\ell}, \quad \Omega = \frac{\omega\ell}{c_T}. \tag{16}$$

The wavelength of the Rayleigh wave Λ is inversely proportional to β such that $\Lambda = 2\pi/\beta$. From the above definitions it may be seen that as $\hat{\beta} \to 0$, then $\Lambda/\ell \to \infty$, or the wavelength cannot "see" the material length ℓ. On the other hand, as $\hat{\beta} \to \infty$ the volume energy length is infinitely larger than the wavelength of the Rayleigh wave. The case $\hat{\beta} = \pi$ corresponds to the shortest physically meaningful wavelength (i.e. $\Lambda \geqslant 2\ell$). Eqs. (14) and (15) represent a plane harmonic wave with varying amplitude functions of the dimensionless coordinate y travelling in the Ox_1-direction and having a dimensionless wave number $\hat{\beta}$, a cyclic frequency ω, and attenuation constants $\hat{\beta}Z_i$ $(i = 1, \ldots, 4)$. Also, Z_a $(a = 1,...,4)$ are given by

$$Z_1^2 = 1 - \left(\frac{\hat{\beta}_1}{\hat{\beta}}\right)^2, \quad Z_2^2 = 1 + \left(\frac{\hat{\beta}_2}{\hat{\beta}}\right)^2,$$
$$Z_3^2 = 1 - \left(\frac{\hat{\beta}_3}{\hat{\beta}}\right)^2, \quad Z_4^2 = 1 + \left(\frac{\hat{\beta}_4}{\hat{\beta}}\right)^2, \tag{17}$$

where $\hat{\beta}_i = \ell\beta_i$ $(i = 1, \ldots, 4)$ and

$$\beta_1 = \frac{1}{2\ell}\sqrt{\sqrt{\left(\frac{c_L}{c_T}\right)^4 + 8\left(\frac{\omega}{c_T}\right)^2\ell^2 + \frac{1}{9}\left(\frac{h\omega}{c_T}\right)^4 - \frac{2}{3}\left(\frac{h\omega}{c_T}\right)^2\left(\frac{c_L}{c_T}\right)^2} - \left(\frac{c_L}{c_T}\right)^2 + \frac{1}{3}\left(\frac{h\omega}{c_T}\right)^2},$$
$$\beta_2 = \frac{1}{\sqrt{2}}\left(\frac{\omega}{\ell c_T \beta_1}\right),$$
$$\beta_3 = \frac{1}{\sqrt{2}\ell}\sqrt{\sqrt{1 + 4\left(\frac{\omega}{c_T}\right)^2\ell^2 - \frac{2}{3}\left(\frac{h\omega}{c_T}\right)^2 + \frac{1}{9}\left(\frac{h\omega}{c_T}\right)^4} - 1 + \frac{1}{3}\left(\frac{h\omega}{c_T}\right)^2},$$
$$\beta_4 = \left(\frac{\omega}{\ell c_T \beta_3}\right). \tag{18}$$

Of considerable importance in this problem is the behavior of the roots (17). The notion of surface waves means that the deformation is confined in a thin layer adjacent to the free surface, i.e. the displacement field is fading exponentially with y, being zero at infinite y, thus

$$\lim_{y \to -\infty} \bar{u}_1 = 0, \quad \lim_{y \to -\infty} \bar{u}_2 = 0. \tag{19}$$

All the roots Z_i $(i = 1,...,4)$ given by Eqs. (17) and (18) are positive real if the following inequality holds true

$$C^2 \leqslant 1 + \hat{\beta}^2, \tag{20}$$

wherein $C = c_R/c_T$, with c_R to be the Rayleigh wave velocity and c_T the shear wave velocity. In the absence of cohesive forces, i.e. $\hat{\beta} = 0$, inequality (20) means that $c_R < c_T$, that is the velocity of Rayleigh surface waves cannot exceed the velocity of shear waves.

The above Eqs. (14) and (15) constitute a homogeneous system of equations in terms of the constants A_1, A_2, A_3 and A_4, which can be put in the compact form $[Y]\{A\} = 0$. To arrive at non-trivial solutions of the homogeneous system, the matrix $[Y]$ must be singular, that is either the determinant of the system must be zero, or one of its four eigenvalues must vanish (eigenvalue problem), i.e.

$$J(\Omega; \hat{\beta}, \nu) = \det([Y]) = 0 \quad \text{or} \quad \lambda_1\lambda_2\lambda_3\lambda_4 = 0, \tag{21}$$

where λ_i $(i = 1,\ldots,4)$ are the four eigenvalues of the 4×4 matrix $[Y]$. This is the Rayleigh determinant for "non-local" elastic surface waves. Then we fix the wave number $\hat{\beta}$, as well as Poisson's ratio, and we consider the equation for the determinant as an equation for the dimensionless frequency Ω. It is not difficult to verify that for $\hat{\beta} = 0$, the determinant equation reduces to the classical Rayleigh function whose roots are given by Eringen and Suhubi [23] for various Poisson's ratios ν. It is also clear that the root of the determinant equation is a function of ℓ, consequently in contrast to the classical theory the Rayleigh wave velocity predicted by the proposed gradient elasticity theory is dispersive.

As it is illustrated in Fig. 5 the various relations among the two length scales ℓ and h lead to different shapes of the dispersion curve. In the same graph the constant relative phase velocity curve predicted by the classical elasticity theory,

$$\frac{c_R}{c_T} = \frac{0.87 + 1.13\nu}{1 + \nu} \tag{21a}$$

is also displayed by a bold curve.

The following observations can be made from the theoretical analysis presented in Fig. 5:

(1) If the strain-gradient length scale ℓ is small compared to the characteristic wavelength of the

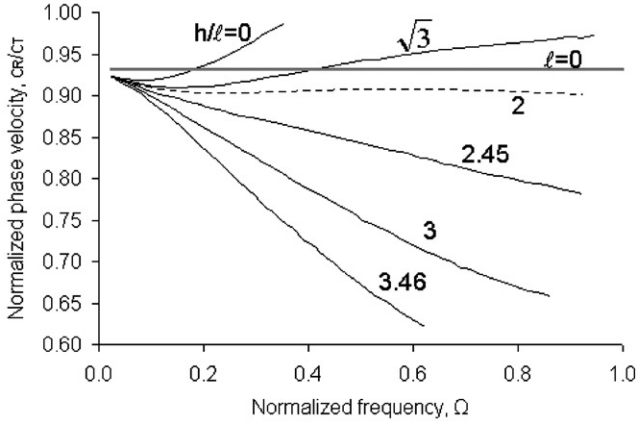

Fig. 5. Effect of the length scale ratio h/ℓ on the form of dispersion curve of Rayleigh waves for $\nu = 0.3$. In the same graph the solution of classical elasticity is shown with a bold line.

Rayleigh wave, that is $\Omega \to 0$, then the results obtained from gradient and classical elasticities coincide.

(2) For $h \leqslant 2\ell$ the dispersion curve initially decreases with the frequency Ω and then increases. The gradient theory predicts larger Rayleigh wave velocities than the classical theory above some value of the dimensionless frequency. On the other hand, for $h \leqslant 2\ell$ the dispersion curve decreases monotonically with Ω and resembles the curve derived from atomic lattice calculations [24].

(3) Measured dispersion curves through carefully performed Rayleigh wave experiments on geomaterials with known mean grain or crystallite size h, Poisson's ratio ν and transverse wave velocity c_T, may be used to establish the strain gradient length scale ℓ.

4. Non-destructive characterization of surface cohesion and damage of Dionysos–Pendelikon marble via surface wave measurements

Surface wave measurements at various frequencies in the range of 100–1000 kHz were performed in the Athens Akropolis Parthenon—that was constructed for the second time in 447–438 BC—in order to develop an acoustic technique for surface wave damage identification and quantification.[1] Measurements were performed in four different classes of stone blocks:

Class 1: Virgin (reference) Dionysos marble which is used for restoration of the monument and it is considered as an undamaged stone.

Class 2: South wall blocks.

Class 3: North wall blocks, which according to the on site archeologists are more damaged than the South wall due to various causes of environmental weathering.

Class 4: East drum blocks. Three blocks were tested, a restored block where major cracks were filled with cement, an unrestored block and a block, which had been exposed to high-temperature variations due to a fire and should be more damaged due to thermal cracking.

A portable acoustic system designed for pulse transmission was used in this experimental study. A schematic drawing of the system is shown in Fig. 6 and it consists of the following units:

(a) Function generator (HP 33120 A).
(b) Power amplifier (ENI Model 2100L).
(c) Digital oscilloscope (Yokogawa DL 1300 A).
(d) Portable lap-top PC for storage of full waveforms.
(e) Acoustic transducers.

The function generator generates an electric pulse, a one-swing sine wave, which is amplified and converted to an acoustic signal by the emitting transducer. The acoustic signal propagates through the sample and is received and converted back to an electrical signal by the receiving transducer. The signal is recorded by a digital oscilloscope, transferred to the lap-top PC and stored on the hard disk. MATLAB has been used for plotting and analysis of the recorded signal. The acoustic signals are recorded by the laptop through an acquisition program written in LABVIEW. The communication between the laptop and the operating units (oscilloscope and function generator) is performed through GPIB transmission lines. The function generator and oscilloscope are controlled through the acquisition program and their settings are stored in the computer together with the acoustic signals.

Transducers for surface wave tests should have a small diameter, such that an accurate estimate of the distance between the emitting and receiving transducer can be made. In addition, the transducers must produce surface waves with enough energy to be detected clearly by the receiving transducer. Different transducers, both commercial and in-house made, were tested and the in-house manufactured transducers were found to be the most suitable ones; see [25] for a detailed description of the selection work. The in-house made transducers contain a piezo-electric disc from Ferroperm A/S in Denmark. They are 5 mm in diameter, 1 mm thick and made by a ceramic called PZT27 (lead zirconium titanate). The frequency of the thickness mode is 1.95 MHz.The transducer backing is 8 mm in diameter and 7 mm in length and made from a mixture of

[1] It is known that the maximum depth of penetration of Rayleigh waves is 2Λ.

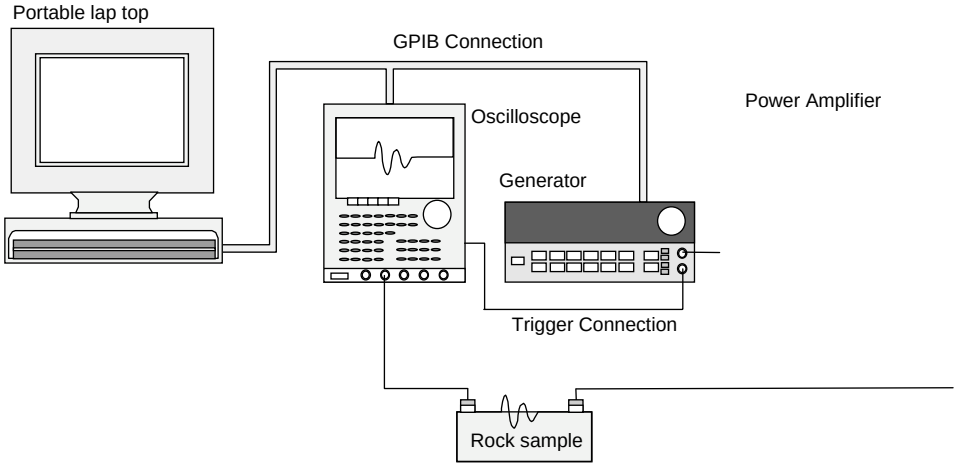

Fig. 6. Schematic of the portable acoustic system.

Fig. 7. Photograph of Dionysos marble blocks (seen to the left) together with the acoustic system. The test was performed on block number two from the front. The other blocks are original marble from the monument. Parts of the South wall are shown in the middle of the photograph.

tungsten particles and epoxy. The backing is covered with conductive silver paint to reduce the electrical noise in the signal. The transducers are not very robust and only a few test series can be performed by a transducer pair. The tests reported in this study are therefore generally performed with different transducer pairs.

A photograph of the acoustic system used in the Athens Akropolis Parthenon is shown in Fig. 7. The computer is seen in the middle of the photograph, placed on top of one of the transporting boxes, while the oscilloscope is seen to the right of the computer. It is placed on top of the function generator, which in turn is placed on top of the amplifier. Neither the function generator nor the amplifier is seen on the photograph. Four blocks of Dionysos marble is seen to the left of the photographs. The remaining blocks are original marble from the Parthenon. Dionysos marble, exhibits very similar properties with Pentelikon marble that was used by the Athenians to build the Parthenon, and it is used currently for the restoration of the Parthenon. It consists of an equidimensional mosaic of fine calcite grains with straight to gently curved boundaries having an average size of $2h \cong 400\,\mu m$. Its representative mineralogical composition by weight is calcite 98%, quartz 0.5%, muscovite 0.5%, sericite 0.5%, chlorite 0.5%, and some small percentage of dolomite may be also present in its composition. This type of quasi-homogeneous rock has a unit weight of 2.67 ($\times 10^5$ N/m^3), porosity 0.371%, and water absorption coefficient by weight 0.11%.

The surface wave velocities found from the tests on each site scatters from test series to test series. However, the general trend should be that the material at each site should have about the same amount of damage. The damping of the signal gives a low ratio between the signal and the noise level, which results in an uncertainty in the picking of the arrival time of the wave. The first break of the surface wave should theoretically be independent of the frequency for a homogeneous linear elastic material. The measured velocities, however, are clearly frequency dependent. The face-to-face tests have shown that the first top of the signal is small compared to its maximum amplitude. Because of damping and noise in the signal, the selection of the first break moves towards the first top. The distance from first break to first top decreases with increasing frequency. A frequency change from 100 to 600 kHz gives thus a decrease of 2.08 μs in arrival time. From the recorded waveforms, the surface wave velocity and its dispersion were calculated. The velocities were calculated using the first break method to find the arrival time t_a. The velocity c_R is given as $c_R = s/t_a$ where s is the distance between the transducers. The velocity was found to differ by 10–50 m/s ($\sim$1.5%) in the waveforms within one-test series for the same source frequency. This could be because the selection of waveform arrivals is affected

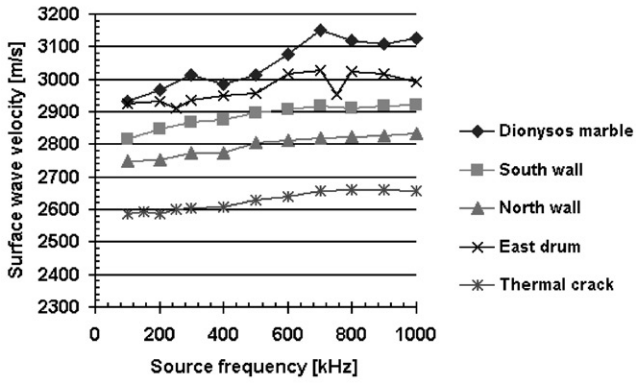

Fig. 8. Mean surface wave velocities versus source frequency at all sites.

Table 1
Best estimations of the strain-gradient length scale and the transverse wave velocity of each class of marble. The estimations of the dynamic shear modulus, crack stiffness, quality factor and damage are also displayed

Marble class	ℓ (mm)	c_T (m/s)	$\tilde{G}$ (GPa)	$\ell\tilde{G}$ ($\times 10^6$ N/m)	Q	D
Dionysos virgin	1.474	3162	26.7	39.4	11.7	0.000
East drum	0.898	3153	26.5	23.8	28.3	0.006
South wall	1.093	3035	24.6	26.9	18.7	0.079
North wall	0.865	2965	23.5	20.3	26.7	0.121
East drum with thermal crack	0.822	2787	20.7	17.0	28.4	0.223

by the quality, the noise and the frequency of the signal, or because the transducers are slightly moved during the measurement. If the transducers are moved 1 mm relatively to each other, which is about 1% for the measurements at Akropolis, the velocity of the recorded surface wave will also change by 1%.

The surface wave velocities at 500 kHz source frequency were found to vary from 2630 m/s in the East drum block transected by thermal fractures, to 3012 m/s in the virgin Dionysos marble as shown in Fig. 8. The same figure shows the mean value of the surface wave velocities for each test site versus source frequency. Note that the velocities found for South Wall tests are higher than the corresponding velocities found for North wall and both are below the velocities found for undamaged material. This corresponds well with the fact that the North wall is expected to be more damaged than the South wall. The velocities found at East drum are higher than the velocities for the North and South walls except for the test on the block with thermal cracks which showed lower velocities, as expected.

The next task is to estimate the values of the transverse wave velocity c_T and internal length scale ℓ of each class of marble. This estimation will be based on the following data:

(i) The transverse wave velocity $c_T = 3160$ m/s of the virgin Dionysos marble [25].
(ii) The dynamic Poisson's ratio $\nu = 0.31$ of the virgin Dionysos marble [25].
(iii) The mean grain size of the calcite crystals of Dionysos marble $2h = 0.4$ mm.
(iv) The dispersion curves displayed in Fig. 8 above.

First, the values of the transverse wave velocity of each type of marble was found by requiring that the normalized wave velocity as $h/\ell \to 0$ should be equal to that predicted by the local linear elasticity theory for a material with Poisson's ratio $\nu = 0.31$, that is $c_R/c_T = 0.928$ for $\Omega \to 0$. In a second step, the values of the gradient length scale ℓ for the five types of marble were found by a constrained non-linear minimization routine of the sum Σ of the squares of differences between the predicted Rayleigh wave velocities $c_{R,i}^{pred}$ from the exposed strain gradient theory above and the measured velocities $c_{R,i}^{meas}$ at each wave frequency ω_i $(i = 1,\ldots,N)$, that is to say

$$\Sigma = \min\left[\sum_{j=1}^{N}(c_{R,j}^{pred} - c_{R,j}^{meas})^2\right] \leqslant \varepsilon, \tag{22}$$

where N is the total number of measurements at the corresponding surface wave frequencies and ε is the prescribed small error tolerance. After best fitting the experimental data with the theoretical model, Table 1 was constructed. In the same table the dynamic shear modulus and damage of the various marble categories that are calculated by employing the following equations are also displayed

$$G = \rho c_T^2, \quad \tilde{G} = \rho \tilde{c}_T^2, \tag{23a}$$

$$D = 1 - \frac{\tilde{G}}{G} = 1 - \frac{\tilde{c}_T^2}{c_T^2}, \tag{23b}$$

in which ρ denotes the density of the material, $\tilde{G}, \tilde{c}_T$ denote the effective dynamic shear modulus and transverse wave velocity of the damaged marble, respectively. The respective quantities without the curly overbar correspond to the virgin undamaged Dionysos marble.

From the above table it is seen that $h/\ell \cong 0.13$–0.25, hence there is no effect of grain size on the dispersion of all classes of marble. Second, it is shown that, despite the fact that both virgin Dionysos marble and East drum test materials have a more or less equal transverse wave velocity and consequently the same level of surface damage, the marble of the East drum is characterized by a much lower cohesion of its superficial layers or microcrack stiffness $G\ell$. Hence, both these parameters should be considered for the characterization of

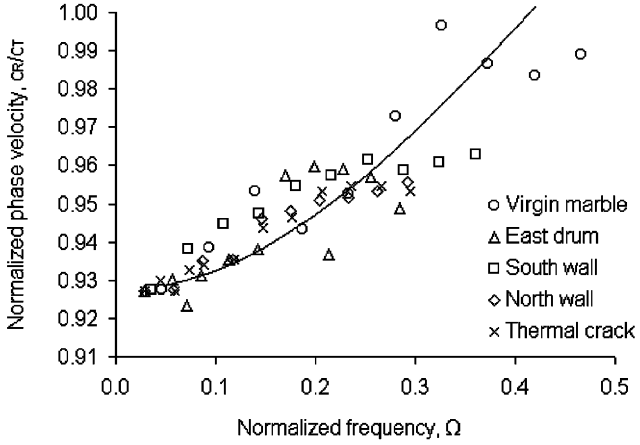

Fig. 9. Dimensionless surface wave velocities versus dimensionless source frequency predicted by gradient elasticity and measured in situ.

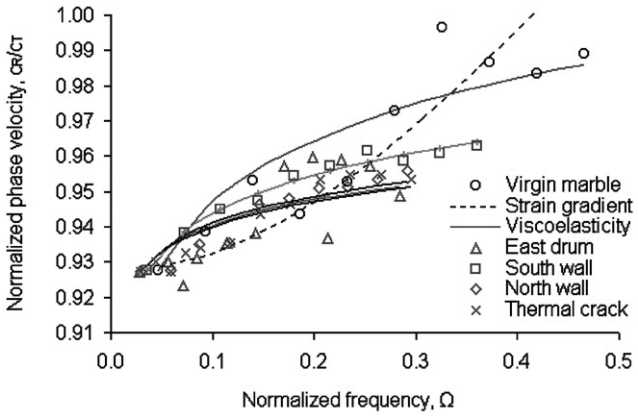

Fig. 10. Best predictions of the measured dispersion curve of each marble class by strain gradient elasticity and viscoelasticity.

mechanical properties of a geomaterial. As it was expected and also noted from the above table, the microcrack stiffness decreases as the damage of marble increases.

Finally, after appropriate normalization of all the test data we have constructed the corresponding dispersion data that are illustrated in Fig. 9. In the same figure the theoretical dispersion curve derived from the proposed theory that corresponds to $h/\ell \cong 0$ is also displayed.[2]

Another explanation for the frequency dependency of the velocity may be given by assuming that the material behaves like a viscoelastic solid. When a mechanical pulse propagates through a viscoelastic solid it is dispersed, as the high-frequency components travel faster and are attenuated more rapidly that those of lower frequency. Kolsky [26] proposed the following expression for the wave velocity $\tilde{c}_R$ as a function of the frequency ω

$$\tilde{c}_R = c_R\left(1 + \frac{\ln\left(\frac{\omega}{\omega_0}\right)}{\pi Q}\right), \tag{24}$$

where ω_0 is a reference frequency and Q is the quality factor of the stone that represents the ratio of stored to dissipated energy. Fitting the data in Fig. 10 for the reference Dionysos marble gives a quality factor $Q = 11.67$. Such a value appears to be rather low for marble. A more representative value should have been an order of magnitude larger, in which case the frequency dependency of the velocity would have been lower. Further, Fig. 10 and Table 1 present the best fitting curves and Q-values, respectively, for the other four marble classes.

Also, from Fig. 11a it may be seen that a linear trend exists separately between (a) the crack stiffness and (b) the quality factor and the damage of marble, although the former has a negative slope and the latter a positive slope, as it was intuitively expected. Although these linear relations have a relatively low correlation coefficient it is worth noticing from Fig. 11b that Q and $G\ell$ are linearly related with a high correlation coefficient.

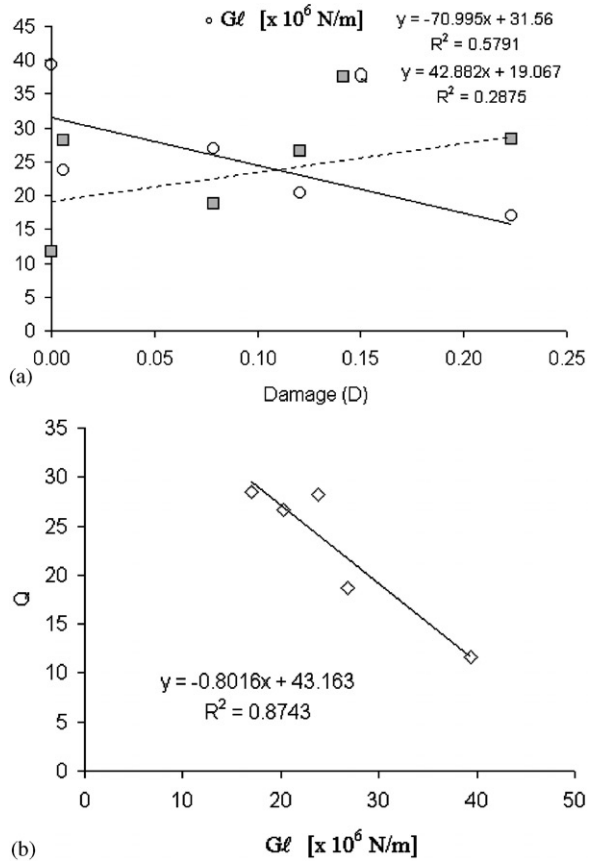

Fig. 11. (a) Dependence of the crack stiffness parameter and quality factor on the damage of Pendelikon marble. (b) Empirical relation of quality factor with crack stiffness parameter of Pendelikon marble.

[2] It may be shown that the dispersion curves for $h/\ell \cong 0.13-0.25$ almost coincide with the curve corresponding to $h/\ell \cong 0$.

5. Conclusions

A new continuum micromechanics theory that takes into account the role of strain gradients is proposed in this work. Subsequently, this theory is applied for the back analysis of in situ surface wave propagation tests at Parthenon. The following main conclusions may be drawn from this theoretical and experimental study:

- Within this formulation, two characteristic internal length scales of the medium are introduced. One of them, ℓ, is associated with an additional term appearing in the strain-energy density expression and accounts for the influence of strain gradients near boundaries (i.e. grain boundaries and microcracks). The other, h, is the characteristic size of the unit cell of the medium (i.e. crystallite of a polycrystalline rock or grain of a granular soil or rock material).
- Also, a new material parameter defined as the product $G\ell$ (G is the shear modulus) has been shown to control the stiffness of a microcrack in a material or alternatively the cohesion of the material surrounding the microcrack.
- It is demonstrated that this theory predicts dispersive Rayleigh waves in contrast to classical Elasticity Theory. Depending on the ratio of material length scales h/ℓ the theory yields increasing or decreasing surface wave phase velocity with frequency. The first case is also predicted by viscoelasticity theory although the dispersion curve is concave downwards (e.g. Fig. 10). The second case resembles very closely that predicted by the atomic lattice theory.
- The back analysis of the surface wave measurements in reference to Dionysos–Pendelikon marble and at various sites in the Athens Akropolis Parthenon with the proposed strain-gradient (microelasticity) theory showed that surface cohesion—that may be expressed with crack stiffness parameter $\ell\tilde{G}$—as well as damage D, can be quantitatively estimated through velocity dispersion tests. It is shown that an approximate linear relation exists between the crack stiffness parameter with damage of the marble. An interesting outcome of the proposed micromechanical theory is that it links the propagation of surface waves with the mechanical behavior of cracked rocks that is depicted by the damage which influences the elastic constants and by the intrinsic length scale ℓ that influences the crack opening displacement and initiation [7]. It is remarked here that the weathering of marble is manifested by both the change of its microfabric at a depth that is reached by the surface waves and some surface alteration (roughness) of the a priori perfectly smooth monumental marble. However, both alterations are manifestations of surface damage of the marble.

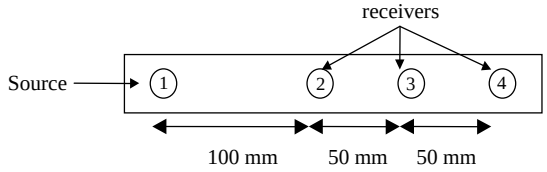

Fig. 12. Proposed acoustic system for surface wave measurements.

- In an alternative fashion, the in situ test results are interpreted with viscoelasticity theory. In this case also the quality factor Q of the four marble classes is correlated linearly with the surface damage of the marble. However, it is remarked that the estimated Q-values appear to be rather low for marble (it varies between 11.7 and 28.5). For rocks the value of Q is found to vary between 30 and 300 [27]. Finally, a very good linear relation of quality factor Q with $\ell\tilde{G}$ is found for the Dionysos–Pendelikon marble.

An improved test method is proposed here based on the above experimental and theoretical results. This method aims to identify cohesion and damage of a stone close to the surface. A set up with one source transducer and three receivers is proposed, as shown in Fig. 12. The transducers should be mounted on line at fixed distances. This allows the calculation of the velocities with better precision and the calculation of the wave attenuation with distance. This configuration allows also the identification of refracted or reflected waves since the waveforms at various distances from the source can be compared. The attenuation is known also to depend on the surface roughness and the proposed test configuration can then give a measure of the surface roughness based on a few tests. The attenuation is also frequency dependent and using different frequencies will give a measure of the size of the surface cracks/inhomogeneities. The transducers should be broad banded and able to measure frequencies between 100 kHz and 1 MHz.Typical frequencies used in a study should be 250, 500 and 750 kHz, which would give a corresponding wavelength of 12, 6 and 4 mm. This will provide the necessary distance between source and receiver in order to avoid near field effects and provide information of the surface up to 12 mm depth in the stone. A test series on a surface should typically consist of tests with minimum three different source frequencies and several tests with the same source center frequency which allow us to stack the data to get rid of noise.

Acknowledgements

This article is a result of research partially supported by funds of the European Union under the contract SMT4-CT96-2130 (1997-2000), as well as of McDUR Project with Contract Number G6RD-CT-2000-00266

of the European Union RESEARCH DG (2001–2004). The authors would also like to thank Prof. I. Vardoulakis and Prof. H. Georgiadis of National Technical University of Athens for valuable discussions during the course of preparation of the present paper.

References

[1] Royer-Carfagni G. Characterization of mechanical properties, damage of natural building stones in historical monuments. 24-months Progress Report, Contract No: SMT4-CT96-2130, 1999.
[2] Mindlin RD. Micro-structure in linear elasticity. Arch Rational Mech Anal 1964;16:51–78.
[3] Vardoulakis I, Exadaktylos G, Aifantis E. Gradient elasticity with surface energy: mode-III crack problem. Int J Solids Struct 1996;33(30):4531–59.
[4] Exadaktylos G, Vardoulakis I, Aifantis E. Cracks in gradient elastic bodies with surface energy. Int J Fracture 1996;79:107–19.
[5] Exadaktylos GE, Aifantis EC. Two and three dimensional crack problems in gradient elasticity. J Mech Beh Mtls 1996;7(2): 93–117.
[6] Vardoulakis I, Exadaktylos GE. The asymptotic solution of anisotropic gradient elasticity with surface energy for a mode-II crack. In: Durban D, Pearson JRA, editors. Non-linear singularities in deformation and flow. IUTAM Symposium: Kluwer Academic publishers, Haifa, Israel, 1997.
[7] Exadaktylos GE. Gradient elasticity with surface energy: mode-I crack problem. Int J Solids Struct 1997;35(5–6):421–56.
[8] Exadaktylos G, Vardoulakis I. Surface instability in gradient elasticity with surface energy. Int J Solids Struct 1998;35(18):2251–81.
[9] Exadaktylos G. Some basic half-plane problems of the cohesive elasticity theory with surface energy. Acta Mech 1999;133:175–98.
[10] Exadaktylos G, Vardoulakis I. Microstructure in linear elasticity and scale effects: a reconsideration of basic rock mechanics and rock fracture mechanics. Tectonophysics 2001;335(1–2):81–110.
[11] Vardoulakis I, Georgiadis HG. SH surface waves in a homogeneous gradient-elastic half-space with surface energy. J Elasticity 1997;47:147–65.
[12] Eringen AC. On differential equations of nonlocal elasticity and solutions of screw dislocation and surface waves. J Appl Phys 1983;54(9):4703–10.
[13] Eringen AC. Vistas of nonlocal continuum physics. Int J Eng Sci 1992;30:1551–65.
[14] Nowinski JL. On the nonlocal aspects of the propagation of Love waves. Int J Eng Sci 1984;22:383–92.
[15] Exadaktylos G, Georgiadis C, Vardoulakis I. Surface wave propagation in a gradient-elastic half-space with surface energy. In: Theocaris PS et al., editors. Proceedings of the Fifth National Congress on Mechanics, vol. 1. Ioannina, Greece, 1998. p. 227–34.
[16] Coulson CA.Waves. Edinburgh and London: Oliver and Boyd, Reprinted 1958.
[17] Exadaktylos G, Stavropoulou M, Papamichos E, Larsen I, Ringstad C. Rayleigh wave propagation in elastic continua: theory and experiment. EUROMECH 419 Colloquium ''Elastic waves in Nondestructive Testing'', 3rd–5th October 2000, Prague, Czech Republic, 2000, in print.
[18] Sulem J, Vardoulakis I, Exadaktylos G. Microstructural effects in stress concentration and fracture problems in rock mechanics. In: Aliabadi MHseries editor, editor. Nonlinear fracture and damage mechanics. Southampton, Boston: WIT Press, 2001. p. 161–99.
[19] Rayleigh L. On waves propagated along the plane surface of an elastic solid. Proc Lond Math Soc 1887;17:4–11.
[20] Currie DK, Hayes MA, O'Leary PM. Viscoelastic Rayleigh waves. Q Appl Math 1977;35:35–53.
[21] Georgiadis HG, Brock LM, Rigatos AP. Transient concentrated thermal/mechanical loading on the faces of a crack in a coupled-thermoelastic solid. Int J Solids Struct 1998;35:1075–97.
[22] Vardoulakis I. Surface waves in a half-space of submerged sand. Earthquake Eng Struct Dyn 1981;9:329–42.
[23] Eringen AC, Suhubi ES. Elastodynamics, vol. II. New York and London: Academic Press, 1975.
[24] Gazis DC, Herman R, Wallis RF. Surface elastic waves in cubic crystals. Phys Rev 1960;119:533–44.
[25] Papamichos E, Larsen I, Ringstad C. Standardizations of the surface instability test, and laboratory and field acoustic tests. In: Characterization of mechanical properties and damage of natural building stones in historical monuments (Monuments), Final Report, European Project SMT4-CT96-2130, 2000.
[26] Kolsky H. The propagation of stress pulses in viscoelastic solids. Philos Mag 1956;1:693–710.
[27] Brady BHG. Dynamic behavior of rock. In: Hudson JA-in-chief, editor. Comprehensive rock engineering ''Principles, practice & projects'', vol. 1. Fundamentals. Oxford: Pergamon Press, 1993. p. 611–25.